Carrier dynamics in ion-implanted semiconductors studied by simulation and observation of terahertz emission

J. Lloyd-Hughes,[a] E. Castro-Camus,[a] M.D. Fraser,[b] H.H. Tan,[b] C. Jagadish[b] and M.B. Johnston[a]

[a]University of Oxford, Department of Physics, Clarendon Laboratory, Parks Road, Oxford, OX1 3PU, United Kingdom;
[b]Department of Electronic Materials Engineering, Research School of Physical Sciences and Engineering, Institute of Advanced Studies, Australian National University, Canberra ACT 0200, Australia

ABSTRACT

We have experimentally measured the terahertz radiation from a series of ion-implanted semiconductors, both from the bare semiconductor surface and from photoconductive switches fabricated on them. GaAs was implanted with As^+ ions, and InGaAs and InP with Fe^+ ions, and all samples were annealed post implantation. An increase in emission power is observed at high frequencies, which we attribute to the ultrafast trapping of carriers. We use a three-dimensional carrier dynamics simulation to model the emission process. The simulation accurately predicts the experimentally observed bandwidth increase, without resorting to any fitting parameters. Additionally, we discuss intervalley scattering, the influence of space-charge fields, and the relative performance of InP, GaAs and InAs based photoconductive emitters.

Keywords: terahertz, far infrared, ultrafast, ion implantation, carrier dynamics

1. INTRODUCTION

Broadband sources of terahertz radiation have enabled terahertz time-domain spectroscopy (THz-TDS) to become a valuable tool in condensed matter physics, with industrial applications including medical and security imaging. The terahertz range of the electromagnetic spectrum spans from 0.1 THz to > 10 THz in frequency ($1\,\mathrm{THz} = 4.1\,\mathrm{meV} = 300\,\mu\mathrm{m} = 33.4\,\mathrm{cm}^{-1}$). The power of THz-TDS lies in the ability to measure directly the conductivity of a material over a broad frequency range, and as a function of time after some photoexcitation process. This has provided insights in a number of areas of research, including the investigation of the energy gap in superconductors[1] and the study of charge carrier dynamics in photoexcited inorganic[2] and organic[3] semiconductors.

Terahertz radiation can be obtained from emitters based on the ultra-fast separation of photo-excited carriers under an electric field, which typically produce single-cycle electromagnetic pulses. Charge separation can be due to differing electron and hole mobilities (the photo-Dember effect), or alternatively may result from an electric field accelerating electrons and holes in opposite directions. In the later case, the electric field can be internal, such as the space-charge (accumulation or depletion) field that exists near the surface of a semiconductor, or externally applied as in a photoconductive switch.[4]

This contribution discusses how shorter duration terahertz pulses can be obtained from photoconductive switch and surface terahertz emitters, by introducing defects into the semiconductor via ion implantation. The motivation for this work was threefold: firstly, shorter terahertz radiation pulses are desirable in order to obtain broader spectra, enabling studies of different physical systems. Secondly, the study of terahertz emission can help to elucidate aspects of ultrafast carrier dynamics, including the enhancement of terahertz emission under a

Further author information:
Web site: www-THz.physics.ox.ac.uk
J.L-H: E-mail: j.lloyd-hughes@physics.ox.ac.uk, Telephone: +44 (0)1865 272339
M.B.J.: E-mail: m.johnston@physics.ox.ac.uk, Telephone: +44 (0)1865 272236

Ultrafast Phenomena in Semiconductors and Nanostructure Materials X, edited by K.-T. Tsen, J.-J. Song, H. Jiang, Proc. of SPIE Vol. 6118, 61180K, (2006) · 0277-786X/06/$15 doi: 10.1117/12.644074

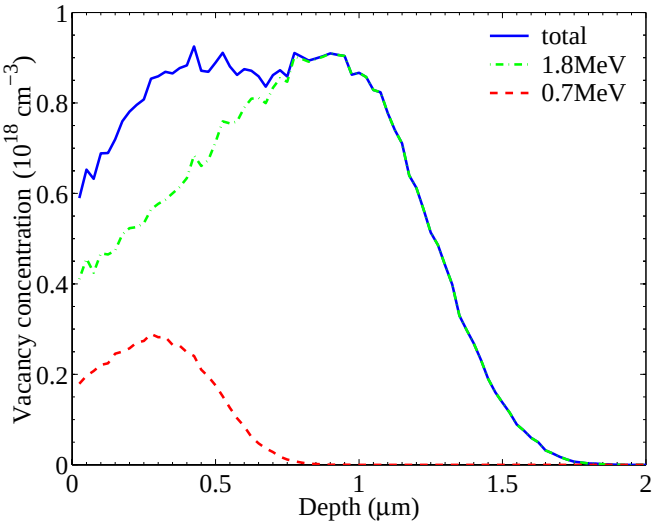

Figure 1. The damage (vacancy) profile of Fe-implanted $In_{0.53}Ga_{0.47}As$ was calculated using the SRIM software,[10] and extends over the absorption depth of 1.55 μm photons ($\sim$ 1.3 μm). Dual-energy (0.7 and 1.8 MeV) implants of Fe^+ ions were performed at room temperature, for different ion doses. The highest dose for the 1.8 MeV implant was 1×10^{16} cm^{-2}, and the other samples had 5% and 0.1% of this dose. The 0.7 MeV implants had 28% of the corresponding 1.8 MeV dose. For the InP:Fe^+ samples 2 MeV and 0.8 MeV implants were used, and for GaAs:As^+ 2.4 MeV and 1.0 MeV, producing similar damage. A post-implantation annealing step (500 °C for 30 minutes) allowed the resistivity to recover. The InGaAs epitaxial layer was 2.5 μm thick, and was grown on a 300 nm thick (undoped) InP buffer layer on a semi-insulating (Fe-doped) InP substrate.

magnetic field,[5–7] and the relative importance of the photo-Dember and surface field charge separation mechanisms in GaAs and InAs.[7,8] Finally, surface emitters can produce the well-collimated THz beams[9] required for many terahertz imaging applications.

In Section 2 we report on the experimentally measured terahertz emission from the surfaces of the ion-implanted semiconductors GaAs:As^+ and $In_{0.53}Ga_{0.47}As$:Fe^+, in which we observe an increase in emitted power at higher frequencies, for samples irradiated with larger ion doses. Similar results are obtained for photoconductive switches made on InP:Fe^+. Subsequently, we discuss how carrier-vacancy momentum scattering and carrier trapping alters THz emission from defect-laden semiconductors, using a semi-classical Monte Carlo simulation (Section 3). This model is able to reproduce the experimentally observed increase in power at high frequencies, without the need for arbitrary fitting parameters (Section 3.3). We then compare the relative simulated performance of InP and GaAs excited by pulses from a 10 fs Ti:Sapphire laser, and $In_{1-x}Ga_xAs$ excited by pulses from a 65 fs Er:fibre laser (Section 3.4), finding that the later could compete with the former in terms of peak emitted power. In Section 3.5 we demonstrate the importance of a fully inclusive approach to the modelling of terahertz emission from photoexcited semiconductors, by showing that the space-charge layer at a semiconductor's surface can alter the emitted electric field from a photoconductive switch. Furthermore, we assess how intervalley scattering can alter terahertz emission.

2. TERAHERTZ EMISSION FROM SEMICONDUCTORS

In order to increase the application of these emitters it is desirable to widen their spectral range. One method of decreasing the pulse duration (and thus broadening the spectrum) is to reduce the electric field decay time after excitation by choosing a semiconductor with a short carrier trapping time and/or a large momentum scattering rate. We obtained such a material using high energy ion implants to create defects to trap and scatter carriers. By using two implants at different energies a uniform damage profile was created, extending over the absorption depth of the semiconductor. Figure 1 illustrates the typical vacancy distribution after implantation and annealing, for InGaAs damaged by Fe ions.

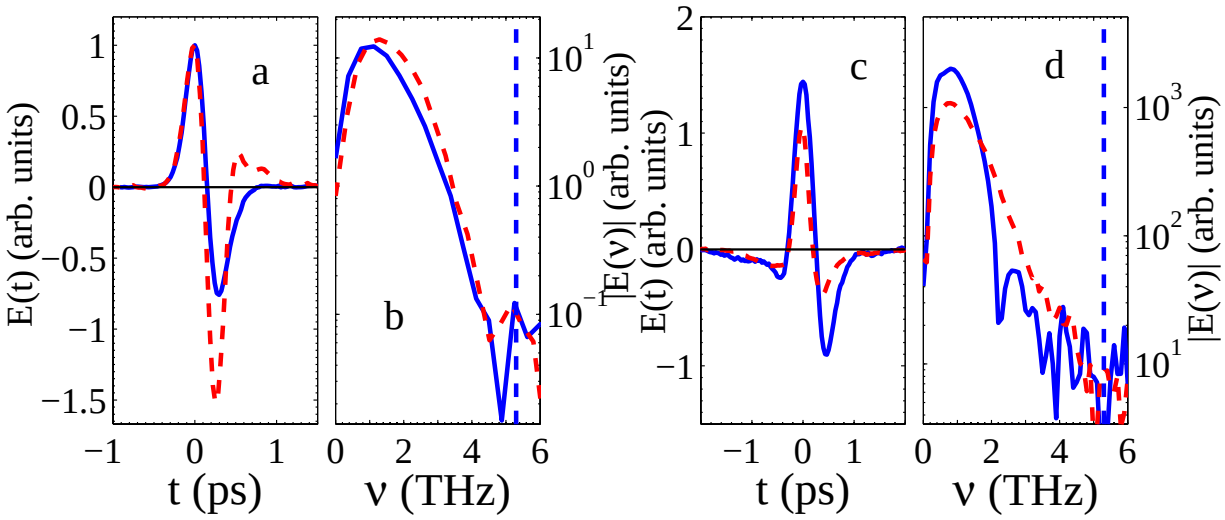

Figure 2. (a) Normalised electric field versus time t from photoconductive switches made on unimplanted InP (solid line) and InP:Fe+ (dashed line) with an incident ion dose at 2.0 MeV (0.8 MeV) of $1 \times 10^{16}\,\mathrm{cm}^{-2}$ ($2.5 \times 10^{15}\,\mathrm{cm}^{-2}$). Measured using a 200 μm $\langle 1\bar{1}0 \rangle$ ZnTe crystal. The peak electric field of the implanted sample is 17× smaller than the peak of the unimplanted. (b) Spectra calculated from a) as a function of frequency ν. (c) Electric field from unimplanted $In_{0.53}Ga_{0.47}As$ (solid line) and Fe-implanted $In_{0.53}Ga_{0.47}As$ (dashed line) with an incident ion dose at 1.8 MeV (0.7 MeV) of $5 \times 10^{14}\,\mathrm{cm}^{-2}$ ($1.4 \times 10^{14}\,\mathrm{cm}^{-2}$). Measured using a 20 μm $\langle 1\bar{1}0 \rangle$ on 1mm $\langle 100 \rangle$ ZnTe crystal. (d) Spectra calculated from c). The dashed vertical lines at 5.2 THz in b) and d) indicate the TO-phonon of ZnTe.

We use a terahertz time-domain spectrometer similar those described in Lloyd-Hughes *et al.*[11] and Johnston *et al.*[12] to measure the terahertz radiation emitted from arsenic-implanted GaAs and Fe-implanted $In_{0.53}Ga_{0.47}As$ surfaces. Additionally, we fabricated photoconductive switches on InP:Fe^+, which were biased with a 20 kHz square wave at ±120 V. Electro-optic sampling (with a 20 μm thick $\langle 1\bar{1}0 \rangle$ ZnTe crystal on a 6 mm $\langle 100 \rangle$ substrate) was used to detect the emitted single-cycle pulse as a function of terahertz pump delay time.

As indicated in Figure 2, greater relative emitted power is obtained at higher frequencies for terahertz emission from Fe-implanted InP photoconductive switches, and Fe-implanted InGaAs surfaces, compared with unimplanted references. This improvement can be attributed to carrier trapping and carrier-defect momentum scattering in the ion-implanted layer. The gain in power at high frequencies comes at the cost of a reduced overall power, owing to the lower mobility of carriers in the damaged layer.

3. SIMULATION OF TERAHERTZ EMITTERS

In order to model the ultrafast carrier dynamics leading to terahertz emission from semiconductor surfaces in such a way that reproduces the experimentally observed features without arbitrary fitting parameters it is appropriate to employ a three-dimensional Monte Carlo simulation, such as presented in Johnston *et al.*[7] This model includes the interactions between extrinsic and photogenerated carriers in the Γ, L and X-valleys, plasmon and magnetoplasmon effects, and the dielectric-air interface. It has been used to distinguish between the diffusion (photo-Dember) and surface field mechanisms of charge separation in InAs and GaAs,[7,9] and to provide a quantitative explanation of the enhancement of THz emission under a magnetic field.[7]

We recently extended this model to simulate photoconductive switches,[13] in which an electric field is applied laterally between two metallic contacts. The emitted power and frequency bandwidth was investigated as a function of bias voltage, pump pulse duration and pump pulse location. The mechanisms limiting the THz power emitted from photoconductive switches were found to fall into two regimes: when illuminated with short duration (< 40 fs) laser pulses the energy distribution of the pump pulse can constrain the emitted power, while for long (> 40 fs) pulses, bias-field screening was found to be the primary power-limiting mechanism.

Table 1. Parameters used in the simulation (at room temperature and pressure), from Vurgaftman *et al.*[15] and the NSM archive.[16] For InGaAs, values of the bowing parameter B for each property are in brackets, taken from Vurgaftman *et al.*[15] When no bowing parameter was found in the literature, linear interpolation between InAs and GaAs was used and the value is given in *italic*. The two-mode TO phonon energies for InGaAs were taken from Groenen *et al.*.[17] For consistency the intervalley deformation potential D_{ij} was taken from Zollner *et al.*,[18] the only reference found with values for GaAs, InAs and InP.

Parameter	GaAs	$In_{0.53}Ga_{0.47}As$	InAs	InP
Γ valley band-gap energy E_Γ (eV)	1.42	0.73 (0.477)	0.354	1.34
L valley offset $E_{L-\Gamma}$(eV)	0.29	0.58 (0.33)	0.73	0.59
X valley offset $E_{X-\Gamma}$(eV)	0.48	0.56 (1.4)	1.02	0.85
Γ valley effective mass (m^*_Γ)	0.067	0.039 (0.0091)	0.022	0.08
L valley effective mass (m^*_L)	0.56	*0.41*	0.29	0.63
X valley effective mass (m^*_X)	0.85	*0.73*	0.64	0.66
Heavy hole effective mass (m^*_{hh})	0.5	0.45 (-0.145)	0.40	0.60
Number of valleys β_Γ, β_L, β_X	1, 4, 3	1, 4, 3	1, 4, 3	1, 4, 3
LO phonon energy (meV)	36.0	*33.0*	30.0	43.0
TO phonon energy (meV)	33.5	*31.6*, *28.3*	26.7	38.1
$D_{\Gamma L}$ (eV/m)	0.4×10^{10}	0.7×10^{10}	1.0×10^{10}	1.8×10^{10}
$D_{\Gamma X}$ (eV/m)	2.9×10^{10}	2.5×10^{10}	2.2×10^{10}	2.6×10^{10}
Acoustic phonon deformation potential (eV)	7.0	*5.9*	5.0	6.0
Speed of sound (ms^{-1})	5240	*4693*	4280	5080
Mass density ρ ($\mathrm{kg\,m}^{-3}$)	5360	*5506*	5667	4810
Static/high frequency dielectric constant ϵ_s, ϵ_∞	12.95, 10.89	13.9 (0.67), *11.6*	15.15, 12.25	12.5, 9.61
Absorption coefficient α ($\mu\mathrm{m}^{-1}$) [$\lambda = 800$nm]	1.2	0.8 [$\lambda = 1.55\mu$m]	6.5	2.5

Additionally, and in agreement with experimental results, the emitted terahertz power was found to be enhanced when the exciting laser pulse was in close proximity to the anode of the photoconductive emitter.[13]

A further advantage of modelling terahertz emitters is that the effect of altering one parameter (or more) of the semiconductor material or laser can be investigated rapidly, and an optimum combination sought. We have identified potential improvements in the power of $In_{1-x}Ga_xAs$ terahertz emitters excited by Er:fibre lasers by choosing alloy fractions closer to InAs.[14]

In this section we describe the setup of the simulation, and how to account for the interaction between terahertz radiation and TO-phonons within a terahertz emitter. We then compare the relative simulated performance of InP and GaAs excited by pulses from a 10 fs Ti:Sapphire laser, and InAs excited by pulses from a 65 fs Er:fibre laser. Subsequently, we discuss the influence of intervalley scattering and space-charge fields on terahertz emission.

3.1. Simulation details

The carrier dynamics model used herein has been described in detail elsewhere.[7, 11, 13, 14] In brief, a set of 10^6 pseudoparticles comprising extrinsic and photogenerated carriers and fixed ions are used to simulate the semiconductor. At each 5 fs step in time the model numerically finds the three-dimensional potential due to the charge density, subject to the appropriate boundary conditions for the surface and Schottky photoconductive switch contacts. The semiconductor is assumed to have a parabolic band structure, and Γ, L and X valleys and heavy holes are included with the parameters listed in Table 1. Carrier-carrier, carrier-phonon, carrier-charged impurity and carrier-vacancy scattering mechanisms are included.[7, 11] The simulated particles are within a box of size $x \times y \times z = 6 \times 6 \times 4\,\mu\mathrm{m}^3$, subdivided into a grid of $64 \times 64 \times 32$ (Figure 3). The contacts of the photoconductive switch are at $-3 \le x \le -1\,\mu$m and $1 \le x \le 3\,\mu$m. A constant bias voltage of 5 V between electrodes was used throughout this work, which corresponds to typical experimental field strengths. The simulation starts at a time $t = -0.7$ ps, to allow the extrinsic carriers to equilibrate before the arrival of the incident pulse, which has peak intensity at time $t = 0.0$ ps, and is centred at $x, y = 0$.

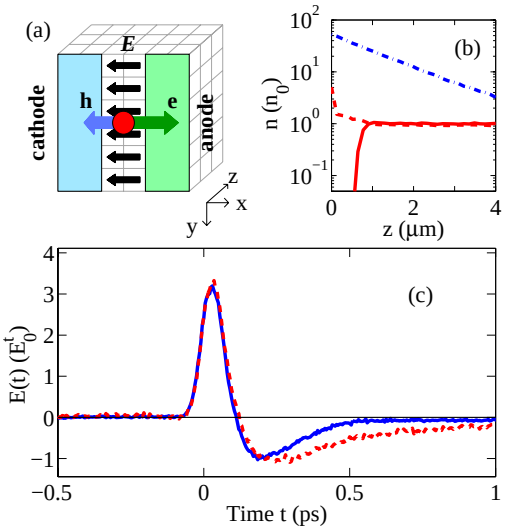

Figure 3. (a) Geometry of the box and grid used in the simulation (see text). (b) Electron density n in model for $In_{0.53}Ga_{0.47}As$ (n-type doping density $1 \times 10^{15}\,cm^{-3}$) as a function of depth z from surface, at $x = 0$ and averaged over y direction. n is in units of $n_0 = 1 \times 10^{15}\,cm^{-3}$. At $t = -0.25\,ps$ the simulated extrinsic electrons are in equilibrium: when the surface pinning potential $V_{pin} = -0.5E_\Gamma$ (defined in Sec. 3.5), a depletion region close to the surface ($z = 0$) can be seen (solid line), while with $V_{pin} = +0.5E_\Gamma$, there is an electron accumulation layer (dashed line). Also plotted is the electron density (dash-dotted line) at $t = 0.00\,ps$, dominated by photoexcited electrons. (c) Simulated E_{THz} calculated from $E_{THz} \propto \partial J_x/\partial t$ for n-type $In_{0.53}Ga_{0.47}As$ with $V_{pin} = -0.5E_\Gamma$ (solid line) and $V_{pin} = +0.5E_\Gamma$ (dashed line), where J_x is the current density in the x direction averaged over the entire box. Parameters typical of a 65 fs Er:fibre laser (laser B) were used, and the coupling between THz radiation and TO phonons in the emitter was not included.

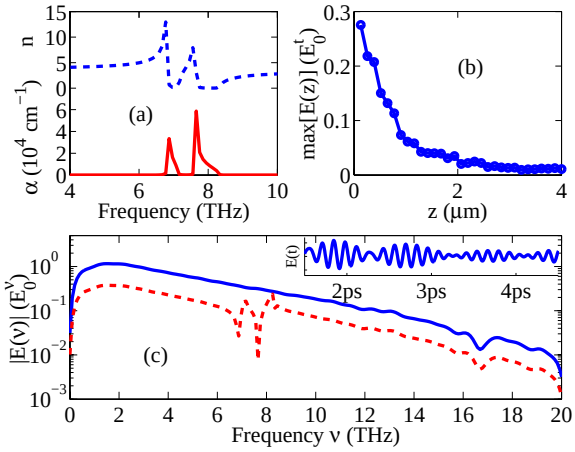

Figure 4. (a) Refractive index n (dotted line) and absorption coefficient α (dashed) calculated from the two TO phonon Drude model form (Eqn. 2) for $In_{0.53}Ga_{0.47}As$. The InAs-like and GaAs-like TO phonon frequencies are $\omega_{1-x}/2\pi = 6.8\,THz$ and $\omega_x/2\pi = 7.6\,THz$. (b) Maximum value of E_{THz} when calculated for each simulation 'slice' in the plane parallel to the semiconductor surface, as a function of depth z from the surface. (c) Effect of propagation on simulated spectra. Spectra of simulated E_{THz} for $In_{0.53}Ga_{0.47}As$ (solid line) from Fig. 3(c) ($\tau_c = 0.3\,ps$, laser B parameters). When Eqn. 1 is used, and E_{THz} is propagated through $0.5\,\mu m$ of $In_{0.53}Ga_{0.47}As$ and into free space the spectrum (dashed line) exhibits characteristic local minima close to the TO phonon frequencies, and local maxima close to the LO-phonon frequencies. (Inset) Damped, beating oscillations are observed in the time-domain.

The simulation uses incident pulse parameters characteristic of two state-of-the-art ultra-short mode-locked lasers: laser A, a 10 fs, $\lambda = 800\,nm$ Ti:Sapphire oscillator, and laser B, a 65 fs $\lambda = 1.55\,\mu m$ Er:fibre laser. We assume a Gaussian spatial and temporal shape, and a transform-limited Gaussian energy distribution for pulses from both lasers. For the case of a 10 fs Ti:Sapphire laser (with central wavelength $\lambda = 800\,nm$, $\Delta\lambda = 80\,nm$, typical beam power $P_{exp} = 400\,mW$ and a repetition rate $R = 75\,MHz$) we use a simulation power of $10\,\mu W$ and a Gaussian spot of standard deviation $\sigma_{x,y} = 0.5\,\mu m$ in order to obtain the same photon flux as experimentally achievable. Amplified Er:fibre lasers have been demonstrated with pulse durations of 65 fs ($\lambda = 1550\,nm$, $\Delta\lambda > 100\,nm$, $P_{exp} = 110\,mW$, $R = 67\,MHz$),[19] while sub-30 fs pulses that are widely tunable over the wavelength range 1130 to 1950 nm may be generated by coupling such Er:fibre laser light into a highly non-linear fibre.[20] For excitation around $1.55\,\mu m$ we use $P = 6\,\mu W$ and $\sigma_{x,y} = 0.5\,\mu m$, chosen to give the same photon flux as for the Ti:Sapphire, so that a comparison between $In_{0.53}Ga_{0.47}As$ switches excited by $1.55\,\mu m$ radiation, and GaAs excited by 800 nm can be made.

3.2. THz pulse propagation within the emitter

The radiated THz electric field E_{THz} was calculated in the far-field approximation from the simulated current density $\mathbf{J}$ using the relation:

$$\mathbf{E}_{\mathrm{THz}} \propto \frac{1}{1+\sqrt{\epsilon}} \frac{\partial \mathbf{J}}{\partial t} \tag{1}$$

where the dielectric function ϵ was modelled using the well-known Drude-Lorentz formula for TO phonon-polaritons.[21] For materials such as $\mathrm{In_{1-x}Ga_xAs}$ that exhibit two TO phonon modes, ϵ is given by:

$$\epsilon_{\mathrm{TO}}(\omega, \mathrm{x}) = \epsilon_{\infty}^{\mathrm{x}} + \frac{\epsilon_{\mathrm{s}}^{\mathrm{x}} - \epsilon_{\mathrm{s}}^{\mathrm{x}}}{1 - \omega^2/\omega_{1-\mathrm{x}}^2 - \mathrm{i}\omega\Gamma/\omega_{1-\mathrm{x}}^2} + \frac{\epsilon_{\mathrm{s}}^{\mathrm{x=1}} - \epsilon_{\infty}^{\mathrm{x}}}{1 - \omega^2/\omega_{\mathrm{x}}^2 - \mathrm{i}\omega\Gamma/\omega_{\mathrm{x}}^2} \tag{2}$$

where ϵ_s^{x}, $\epsilon_{\infty}^{\mathrm{x}}$ are the low and high frequency dielectric constants at alloy fraction x. The angular frequency of the GaAs-like (InAs-like) TO phonon is ω_{x} ($\omega_{1-\mathrm{x}}$). The damping rate was assumed to be $\Gamma = 0.06\,\mathrm{ps}^{-1}$ for both InAs-like and GaAs-like TO phonon modes.[21] In order to estimate the thickness of semiconductor through which the emitted THz must propagate we calculated the maximum THz electric field from each 'slice' parallel to the surface. Taking the mean of this distribution results in a weighted propagation thickness of $\sim 0.5\,\mu$m. Assuming that the emitted THz radiation is collected in the reflection geometry (to minimise absorption and dispersion in the semiconductor material[22]), $0.5\,\mu$m is a reasonable estimate of the propagation distance of THz radiation in an InGaAs photoconductive switch. We therefore propagate E_{THz} through this thickness of semiconductor, and into free space, resulting in a characteristic reduction in spectral amplitude of emitted THz radiation close to a TO phonon mode, and an enhancement just above the frequency of an LO phonon (as seen in Fig. 4).

3.3. Simulation of GaAs:As$^+$ surface emitters

Carrier-vacancy momentum scattering is included in the simulation by assuming that carriers scatter elastically from an electrically neutral spherical square well.[11] This model produces typical scattering rates up to $\sim 10^{14}\,\mathrm{s}^{-1}$ at the vacancy concentrations expected for the highest dose samples, $N_{\mathrm{vac}} = 1 \times 10^{18}\,\mathrm{cm}^{-3}$. At these concentrations the emitted electric field duration is shortened somewhat, but not significantly enough to account for the observed change in spectral shape.[11]

The effect of carrier trapping at defect sites was included in our simulation by introducing an exponential decay of the number of photoexcited carriers n as a function of time t after the infrared pulse according to the equation $n(t) = n(0)e^{-t/\tau_{\mathrm{c}}}$. The carrier lifetime τ_{c} of our ion-implanted samples has been measured by time-resolved photoluminescence[23–26] to be as short as 100 fs and 130 fs for the highest dose GaAs:As$^+$ and InP:Fe$^+$ samples respectively. We have confirmed the sub-picosecond carrier lifetimes of our ion-implanted samples via optical-pump, terahertz probe experiments.[27,28]

As indicated by Figure 5, the simulated change in the frequency of peak terahertz emission at different values of τ_{c} closely follows the measured change. Similar changes in spectral shape with carrier lifetime can be observed in the simulation of InGaAs:Fe$^+$ photoconductive switches,[14] and this model is also applicable to terahertz emission from low-temperature-grown semiconductors.

3.4. Comparison of InP, GaAs and InAs terahertz emitters

In Fig. 6 we compare the simulated E_{THz} for InP and GaAs photoconductive switches excited by 10 fs pulses from laser A with that obtained for InAs excited by 65 fs pulses from laser B. These parameters were chosen to enable a comparison between THz systems based on current state-of-the-art lasers. In order to enable a comparison between the results presented we normalize E_{THz} in the time and frequency domains to the peak simulated values for a GaAs photoconductive switch excited by laser A (with carrier trapping time $\tau_{\mathrm{c}} = 100\,\mathrm{ps}$), denoted E_0^t and E_0^ν respectively. Similarly the emitted THz power (defined as the square of $E_{\mathrm{THz}}(t)$ integrated over all times) is normalized to P_0, the power for the GaAs emitter.

The peak value of E_{THz} for InAs is larger than for GaAs, despite the Er:fibre laser's power being lower than that of the Ti:Sapphire (the photon flux is the same for both lasers). This can be attributed in part to more incident photons having an above-bandgap energy. As the inset of Fig. 6 indicates, almost 100% of photons from

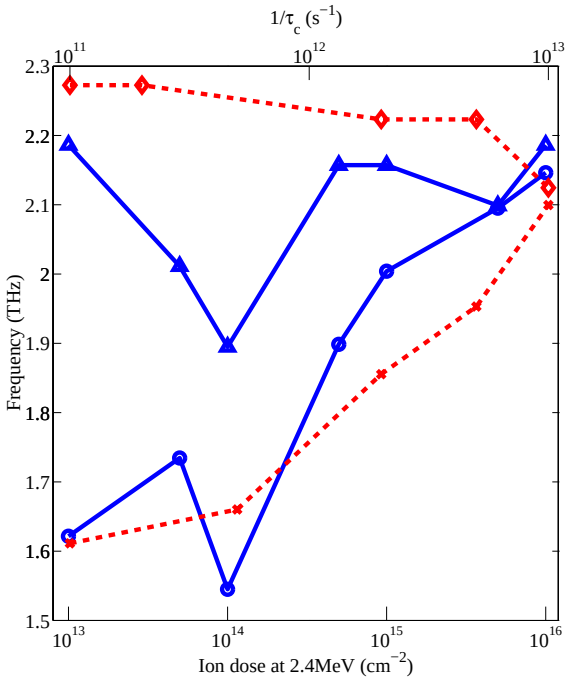

Figure 5. Frequency of peak emitted THz power f_{p} (circles, solid line) and FWHM of spectra (triangles, solid line) as a function of ion dose at 2.4 MeV (the 1 MeV ion dose was a quarter of the 2.4 MeV dose). f_{p} is defined as the midpoint of the two frequencies at which the amplitude of the Fourier transform of the electric field is 95% of its maximum. The experimental data can be compared with values extracted from spectra produced by our carrier dynamics simulation (dashed lines), plotted as a function of inverse carrier trapping time $1/\tau_{\mathrm{c}}$. The trend in f_{p} (crosses) from the simulation reproduces the experiment. The FWHM from the simulation (diamonds) do not vary with $1/\tau_{\mathrm{c}}$, and are consistent with those measured. The simulated spectra have had a high-pass and low-pass filter applied to them, to account for the effect of the parabolic mirrors and ZnTe detection crystal.[11]

laser B have energy greater than $E_\Gamma(\mathrm{InAs}) = 0.35\,\mathrm{eV}$, while the above-bandgap fraction for laser A is smaller (∼80%). The fact that InAs has a lower effective mass in the Γ-valley than GaAs also contributes to the power increase. Qualitatively, a smaller effective mass produces a larger mobility $\mu = e\tau/m^*$, which should result in a larger transient current and therefore power. However, this argument neglects changes in the carrier scattering time τ, and we discuss this point further in.[14]

Turning now to E_{THz} for InP, we observe a slightly greater peak time-domain and spectral amplitude than for GaAs, despite the larger m^*_Γ (lower mobility) of InP. This is again related to the energy distribution of the incident infrared pulses. Defining the excess energy of the incident pulse as $\Delta = E_\gamma - E_\Gamma$ we see that $\Delta = 0.21\,\mathrm{eV}$ for InP, while $\Delta = 0.13\,\mathrm{eV}$ for GaAs. A greater percentage of incident photons are therefore absorbed in InP (∼91%) than GaAs (80%), contributing to a larger E_{THz}.

3.5. Intervalley scattering

A few of the semiconductor parameters that are less well known experimentally could influence the simulation results reported here, and we therefore assess in this section how varying their value alters the modelled electric field. One such parameter is the intervalley deformation potential D_{ij}, the characteristic strength of intervalley electron-phonon scattering, in which an electron absorbs or emits a near zone-edge phonon and transfers to another valley. The momentum scattering rate $W_{ij}(k)$ used in the simulation is:[29, 30]

$$W_{ij}(k) = \frac{\pi\beta_j D_{ij}^2}{\omega_j \rho} N(E_{\mathbf{k}} \pm \hbar\omega_j - E_{j-i}) \left(f_B(\hbar\omega_j) + \frac{1}{2} \mp \frac{1}{2} \right) \tag{3}$$

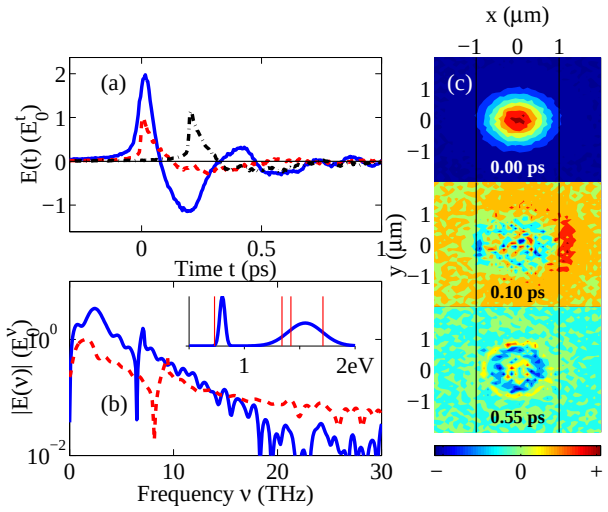

Figure 6. (a) Simulated E_{THz} for GaAs (dashed line) and InP (dash-dotted line, offset in time by +0.2 ps for clarity) photoconductive switches excited by laser A, and InAs (solid line) excited by laser B. Both InP and InAs have a larger peak E_{THz} than GaAs. (b) Fourier transform of E_{THz} (t) from (a), for InAs (solid) and GaAs (dashed line). The spectrum for InP (not shown) is substantially the same as that for GaAs (with its TO phonon absorption at 9.2 THz). (Inset) Schematic energy distributions of a transform-limited 65 fs pulse at λ =1.55 μm (0.8 eV) and a 10 fs pulse at λ =800 nm (1.55 eV). Vertical lines at 0.73 eV, 1.34 eV, 1.42 eV and 1.71 eV respectively indicate E_Γ for $In_{0.53}Ga_{0.47}As$, InP and GaAs, and E_L for GaAs. (c) Change in electron density between simulation time steps in the plane of the surface $(x-y)$, averaged over the depth z (see text for discussion). The black lines at $x=-1\,\mu$m and $x=1\,\mu$m mark the positions of the cathode and anode.

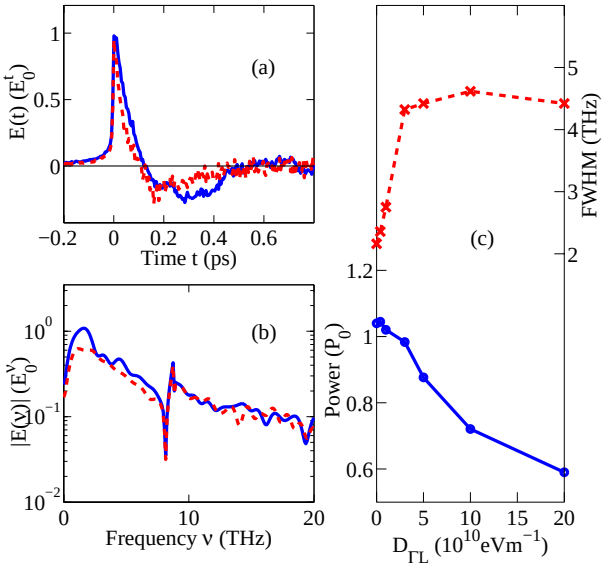

Figure 7. Simulated THz electric field from GaAs as a function of intervalley deformation potential $D_{\Gamma L}$. (a) Simulated E_{THz} for $D_{\Gamma L}=0$ (solid line) and $D_{\Gamma L}=2.0\times10^{11}\,\mathrm{eVm^{-1}}$ (dashed line), and (b) shows the Fourier transform of (a). In (c) the power (circles) and FWHM (crosses) for simulations run as a function of $D_{\Gamma L}$ are given. Laser parameters A (10 fs Ti:Sapphire) were used.

where i and j represent the initial and final valleys (e.g. Γ and L), $E_{\mathbf{k}}$ is the electron's kinetic energy above the valley's minimum, and $f_B(\hbar\omega_j)$ is the Bose-Einstein distribution function. ω_j is the angular frequency of zone-edge phonons, where it has been assumed in the derivation of Eqn. 3 that TO and LO phonon modes have the same (wavevector independent) frequency. The density of final electron states is N, and the other symbols are as defined in Table 1.

There is a considerable range in the values of D_{ij} reported in the literature: even for well characterized semiconductors such as GaAs the reported values of $D_{\Gamma-L}$ range from $0.4\times10^{10}\,\mathrm{eVm^{-1}}$ (theoretically calculated from a rigid ion pseudopotential method[18]) to $1\times10^{11}\,\mathrm{eVm^{-1}}$ (measured using the Gunn effect), and $7\times10^{10}\,\mathrm{eVm^{-1}}$ (using non-equilibrium phonon spectroscopy).[31,32] So as to assess how this uncertainty may affect our simulation results, we plot in Fig. 7 the simulated E_{THz} for GaAs excited by laser A as a function of $D_{\Gamma-L}$. As $D_{\Gamma-L}$ increases the THz pulse shortens (and the emitted THz power decreases) because of the higher $\Gamma-L$ scattering rate. The increase in $D_{\Gamma-L}$ from $0.4\times10^{10}\,\mathrm{eVm^{-1}}$ to $1.0\times10^{10}\,\mathrm{eVm^{-1}}$ towards x=0 in $In_{1-x}Ga_xAs$ therefore counteracts the overall rise in power obtained due to a higher electron mobility.[14] However, even if $D_{\Gamma-L}$ happened to vary between $0.4\times10^{10}\,\mathrm{eVm^{-1}}$ and $2.0\times10^{11}\,\mathrm{eVm^{-1}}$ from x=1 to x=0, Fig. 7 suggests that the power drop due to increased intervalley electron-phonon scattering (reduced to $\sim60\%$) would not counterbalance the rise in power ($\sim400\%$). The FWHM are approximately constant for $D_{\Gamma-L}\geq3\times10^{10}\,\mathrm{eVm^{-1}}$, and while there is a noticeable decrease in FWHM below this value (because of the appearance of the spectral peak near

2 THz, associated with plasma oscillations) the spectral shape does not dramatically change.

3.6. Surface space-charge layer

A second parameter that is not typically well known is the value of the surface field pinning potential. At a semiconductor surface singly occupied atomic orbitals (dangling bonds) create surface states that pin the Fermi level at an energy $V_{\rm pin}$, and these states create an electric field near the surface. A change in $V_{\rm pin}$ cannot directly alter the THz emission from a photoconductive switch, since dipoles formed by charges separating under a surface field cannot radiate in the direction perpendicular to the surface (the z direction in Fig. 3). However, a different surface field could arguably alter the charge carrier distribution, thereby affecting terahertz emission. This is indeed the case, as Fig. 3c indicates.

Difficulties in ensuring clean, oxide-free surfaces make the accurate measurement of $V_{\rm pin}$ challenging. In GaAs $V_{\rm pin} \simeq -0.5E_\Gamma = -0.7\,{\rm eV}$ (relative to the Γ valley minimum), and there is an electron depletion field near the surface. In contrast, for InAs $V_{\rm pin} \simeq 0.1\,{\rm eV}$ (i.e. at the surface the conduction band is below the Fermi level), and an electron accumulation region forms.[33] Accordingly, we varied the pinning potential in the range $-0.5 \leq V_{\rm pin}/E_\Gamma \leq 0.5$ for $In_{1-x}Ga_xAs$, and found a small change in the simulated $E_{\rm THz}$. In Fig. 3(b) the depletion (accumulation) region formed when $V_{\rm pin} = -0.5E_\Gamma$ ($V_{\rm pin} = +0.5E_\Gamma$) for $In_{0.53}Ga_{0.47}As$ is shown, and Fig. 3(c) shows the corresponding simulated $E_{\rm THz}$ for $\tau_{\rm c} = 0.3\,{\rm ps}$. When $V_{\rm pin} < 0$ (i.e. depletion region) the emitted THz pulse is slightly shorter in duration than when $V_{\rm pin} > 0$ (accumulation region). The spectra (not shown) are substantially the same, except for a reduction in spectral power at low frequency (<1 THz) for the shorter duration pulse. The mean scattering rate of electrons in the Γ valley was found to be lower for $V_{\rm pin} > 0$, due to a reduction in the electron-hole scattering rate $W_{\rm e-h}$. This can be attributed to a higher electron density near the surface for an accumulation field, since $W_{\rm e-h} \sim 1/n$.[29,30] The power when $V_{\rm pin} = +0.5E_\Gamma$ was found to be $\sim 1.2\times$ the power at $V_{\rm pin} = -0.5E_\Gamma$, i.e. as the $In_{1-x}Ga_xAs$ alloy approaches InAs the increase in emitted power owing to the higher electron mobility[14] should be further enhanced by the presence of an accumulation region near the surface.

4. CONCLUSION

In summary, we have demonstrated improvements in the power of emitted terahertz radiation from ion-implanted semiconductors, at high frequencies (> 1 THz). This bandwidth increase was related to the ultrafast trapping of carriers on sub-picosecond timescales, and was modelled using a carrier dynamics simulation. The influences of the surface space-charge layer and of intervalley scattering on terahertz emission were also discussed using the simulation.

ACKNOWLEDGMENTS

The authors would like to thank the EPSRC and the Royal Society (UK) for financial support of this work. E.C.C. wishes to thank CONACyT (México) for financial support.

REFERENCES

1. M. C. Nuss, K. W. Goossen, J. P. Gordon, P. M. Mankiewich, M. L. O'Malley, and M. Bhushan, "Terahertz time-domain measurement of the conductivity and superconducting band gap in niobium," *J. Appl. Phys.* **70**, p. 2238, 1991.
2. R. Huber, F. Tauser, A. Brodschelm, M. Bichler, G. Abstreiter, and A. Leitenstorfer, "How many-particle interactions develop after ultrafast excitation of an electron-hole plasma," *Nature* **414**, p. 286, 2001.
3. E. Hendry, J. Schins, L. P. Candeias, L. D. A. Siebbeles, and M. Bonn, "Efficiency of exciton and charge carrier photogeneration in a semiconducting polymer," *Phys. Rev. Lett.* **92**(19), p. 196601, 2004.
4. P. Smith, D. Auston, and M. Nuss, "Subpicosecond photoconducting dipole antennas," *IEEE J. Quantum Electron.* **24**, p. 255, Feb. 1988.
5. A. Corchia, R. McLaughlin, M. B. Johnston, D. M. Whittaker, D. D. Arnone, E. H. Linfield, A. G. Davies, and M. Pepper, "Effects of magnetic field and optical fluence on terahertz emission in gallium arsenide," *Phys. Rev. B* **64**, p. 205204, Nov. 2001.

6. M. B. Johnston, D. M. Whittaker, A. Corchia, A. G. Davies, and E. H. Linfield, "Theory of magnetic field enhancement of surface field terahertz emission," *J. Appl. Phys.* **91**, pp. 2104–2106, Feb. 2002.
7. M. B. Johnston, D. M. Whittaker, A. Corchia, A. G. Davies, and E. H. Linfield, "Simulation of terahertz generation at semiconductor surfaces," *Phys. Rev. B* **65**, p. 165301, Mar. 2002.
8. J. N. Heyman, N. Coates, A. Reinhardt, and G. Strasser, "Diffusion and drift in terahertz emission at GaAs surfaces," *Appl. Phys. Lett.* **83**(26), pp. 5476–5478, 2003.
9. M. B. Johnston, A. Dowd, R. Driver, A. G. Davies, and E. H. L. amd D. M. Whittaker, "Emission of collimated THz pulses from photo-excited semiconductors," *Semicond. Sci. Technol.* **19**, pp. S449–S451, Apr. 2004.
10. J. F. Ziegler and J. P. Biersack, "SRIM 2003 software." Available online at http://www.srim.org.
11. J. Lloyd-Hughes, E. Castro-Camus, M. D. Fraser, C. Jagadish, and M. B. Johnston, "Carrier dynamics in ion-implanted GaAs studied by simulation and observation of terahertz emission," *Phys. Rev. B* **70**, p. 235330, Dec. 2004.
12. M. B. Johnston, L. M. Herz, A. L. T. Khan, A. Köhler, A. G. Davies, and E. H. Linfield, "Low-energy vibrational modes in phenylene oligomers studied by THz time domain spectroscopy," *Chem. Phys. Lett.* **377**, pp. 256–262, Aug. 2003.
13. E. Castro-Camus, J. Lloyd-Hughes, and M. B. Johnston, "Three-dimensional carrier-dynamics simulation of terahertz emission from photoconductive switches," *Phys. Rev. B* **71**, 2005.
14. J. Lloyd-Hughes, E. Castro-Camus, and M. B. Johnston, "Simulation and optimisation of terahertz emission from InGaAs and InP photoconductive switches," *Sol. Stat. Comm.* **136**, p. 595, Dec. 2005.
15. I. Vurgaftman, J. R. Meyer, and L. R. Ram-Mohan, "Band parameters for III–V compound semiconductors and their alloys," *Journal of Applied Physics* **89**(11), pp. 5815–5875, 2001.
16. "NSM semiconductor archive."
17. J. Groenen, R. Carles, G. Landa, C. Guerret-Piecourt, C. Fontaine, and M. Gendry, "Optical-phonon behavior in $Ga_{1-x}In_xAs$: The role of microscopic strains and ionic plasmon coupling," *Phys. Rev. B* **58**(16), pp. 10452–10462, 1998.
18. S. Zollner, S. Gopalan, and M. Cardona, "Microscopic theory of intervalley scattering in GaAs: k dependence of deformation potentials and scattering rates," *J. Appl. Phys.* **68**(4), p. 1682, 1990.
19. F. Tauser, A. Leitenstorfer, and W. Zinth, "Amplified femtosecond pulses from an Er:fiber system: Nonlinear pulse shortening and self-referencing detection of the carrier-envelope phase evolution," *Opt. Expr.* **11**(6), p. 594, 2003.
20. F. Tauser, F. Adler, and A. Leitenstorfer, "Widely tunable sub-30-fs pulses from a compact erbium-doped fiber source," *Opt. Lett.* **29**(5), p. 516, 2004.
21. P. Y. Yu and M. Cardona, *Fundamentals of Semiconductors*, Springer, 3rd ed., 2003.
22. Y. C. Shen, P. C. Upadhya, E. H. Linfield, H. E. Beere, and A. G. Davies, "Ultrabroadband terahertz radiation from low-temperature-grown GaAs photoconductive emitters," *Appl. Phys. Lett.* **83**, p. 3117, Oct. 2003.
23. A. Krotkus, S. Marcinkevicius, J. Jasinski, M. Kaminska, H. H. Tan, and C. Jagadish, "Picosecond carrier lifetime in GaAs implanted with high doses of As ions: An alternative material to low-temperature GaAs for optoelectronic applications," *Appl. Phys. Lett.* **66**(24), p. 3304, 1995.
24. S. Marcinkevicius, C. Jagadish, H. H. Tan, M. Kaminska, K. Korona, R. Adomavicius, and A. Krotkus, "Influence of annealing on carrier dynamics in as ion-implanted epitaxially lifted-off GaAs layers," *Appl. Phys. Lett.* **76**(10), pp. 1306–1308, 2000.
25. C. Carmody, H. H. Tan, C. Jagadish, A. Gaarder, and S. Marcinkevicius, "Ultrafast carrier trapping and recombination in highly resistive ion implanted inp," *J. Appl. Phys.* **94**(2), pp. 1074–1078, 2003.
26. C. Carmody, H. H. Tan, C. Jagadish, A. Gaarder, and S. Marcinkevicius, "Ion-implanted $In_{0.53}Ga_{0.47}As$ for ultrafast optoelectronic applications," *Appl. Phys. Lett.* **82**(22), pp. 3913–3915, 2003.
27. M. C. Nuss, D. H. Auston, and F. Capasso, "Direct subpicosecond measurement of carrier mobility of photoexcited electrons in gallium arsenide," *Phys. Rev. Lett.* **58**(22), pp. 2355–2358, 1987.

28. M. C. Beard, G. M. Turner, and C. A. Schmuttenmaer, "Subpicosecond carrier dynamics in low-temperature grown GaAs as measured by time-resolved terahertz spectroscopy," *J. Appl. Phys.* **90**(12), pp. 5915–5923, 2001.
29. *Numerical Simulation of Submicron Semiconductor Devices*, ch. 2.5. Artech House Inc., Boston, 1993.
30. B. K. Ridley, *Quantum Processes in Semiconductors*, ch. 4.3. Clarendon Press, Oxford, 1999.
31. C. L. Collins and P. Y. Yu, "Generation of nonequilibrium optical phonons in GaAs and their application in studying intervalley electron-phonon scattering," *Phys. Rev. B* **30**(8), p. 4501, 1984.
32. D.-S. Kim and P. Y. Yu, "Hot-electron relaxations and hot phonons in GaAs studied by subpicosecond raman scattering," *Phys. Rev. B* **43**(5), p. 4158, 1991.
33. S. Ono, M. Takeuchi, and T. Takahasi, "Kelvin probe force microscopy on InAs thin films grown on GaAs giant step structures formed on .110. GaAs vicinal substrates," *Appl. Phys. Lett.* **78**(8), p. 1086, 2001.